Proceeding of the IEEE
International Conference on Robotics and Biomimetics
Dali, China, December 2019

# Closed Loop Control of a Continuum Surgical Manipulator for Improved Absolute Positioning Accuracy*

Qi Li[1], Haozhe Yang[1], Yuyang Chen[2] and Kai Xu[1], *Member, IEEE*
[1]*State Key Laboratory of Mechanical System and Vibration*
*School of Mechanical Engineering*
[2] *RII Lab (Lab of Robotics Innovation and Intervention)*
*UM-SJTU Joint Institute*
*Shanghai Jiao Tong University, Minhang, Shanghai Province, China*

{liqi362202, silence1004, supandoria and k.xu}@sjtu.edu.cn

***Abstract* - Robotic assistance in MIS (Minimally Invasive Surgery) has attracted worldwide attention in the past decades. Even though majority of the implemented robotic surgical manipulators have articulated structures, continuum structures have been more widely applied due to their advantages of intra-abdominal dexterity and safe interaction with anatomy. However, absolute positioning accuracy of a continuum surgical manipulator can be low due to its nonlinear bending behaviors under different loads and un-modeled manufacturing clearance. This paper hence presents a proof-of-concept investigation of closed loop control scheme for improving the manipulator's absolute positioning accuracy. System descriptions, kinematics modeling and experimental validations are reported in detail to demonstrate the effectiveness of the proposed control scheme.**

***Index Terms* – closed loop control, continuum surgical manipulator, absolute positioning accuracy.**

## I. INTRODUCTION

Robotic assistance has attracted worldwide attention in the past decades to facilitate MIS (Minimally Invasive Surgery) laparoscopy, in order to better realize the benefits of MIS in terms of reduced trauma, quicker recovery and lower complication rate [1].

While articulated manipulators are mostly used in the existing robotic surgical systems, continuum structures are more and more widely adopted due to the intra-abdominal dexterity and inherent safety [2]. These continuum surgical manipulators usually have several distal DoFs (Degree of Freedom) for spatial movements in a patient's body cavity [3-5].

When a robotic surgical manipulator is inserted into a patient's body cavity for surgical manipulation, accurate positioning control plays a crucial role in assisting surgeons in precisely reaching nidus and accomplishing surgical operations. Unlike the approach where an articulated external patient-side manipulator maneuvers a stick-like surgical instrument using closed loop control and model-based feedforward robot dynamics, continuum manipulators usually operate without shape feedback information. Absolute positioning accuracy of continuum surgical manipulators hence can be low due to their nonlinear bending behaviors under different loads and un-modeled manufacturing clearance.

Although it has been shown that the accuracy of segment bending can be substantially improved from motion calibration to account for friction and actuation hysteresis [4, 6, 7], alternative approaches are still in need to compensate the motion errors when the manipulator is under significant external loads. Hence, this paper presents a proof-of-concept investigation of closed loop control of a continuum manipulator for improving the manipulator's absolute positioning accuracy.

Tip position feedback of a continuum manipulator can be acquired using electromagnetic (EM) sensors for position control [8] and even stiffness control [9]. However, EM sensors are often sensitive to electromagnetic interference (e.g., from metal surgical tools), which narrows their uses in surgical applications.

The tip position feedback is also possible to achieve via optical tracking. The effectiveness has been demonstrated in model-less [10] and model-based approaches [11, 12]. Since laparoscopic surgical robotic systems always operate under vision guidance, visual feedback for tip position may be an ideal way to achieve closed loop control [13]. Due to the algorithmic complexity and possible feedback accuracy issues, an optical tracking approach based on near IR (infrared) light was adopted in this proof-of-concept investigation as shown in Fig. 1, where the markers were attached to the tip and the base of a continuum manipulator for the goal of achieving accurate closed loop position control.

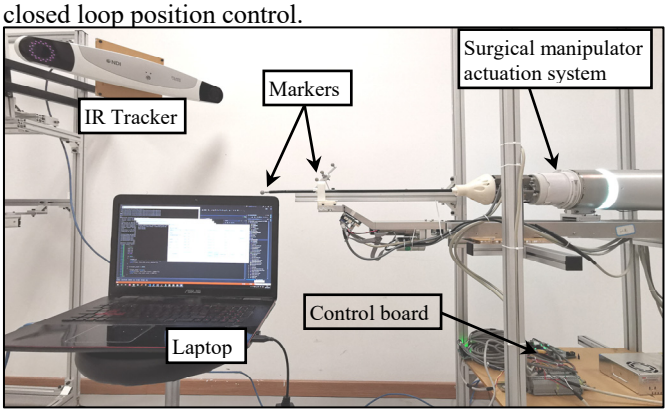


Fig 1. Setup of the closed loop control of a continuum surgical manipulator, including the maniplator and an optical tracking system.

* This work was supported in part by the National Key R&D Program of China (Grant No. 2017YFC0110800), and in part by the National Natural Science Foundation of China (Grant No. 51722507, Grant No. 51435010 and Grant No. 91648103).



978-1-7281-6321-5/19//$31.00 ©2019 IEEE

The rest of this paper is organized as follows. Section II presents the topology, nomenclature, forward kinematics and actuation kinematics of the continuum surgical manipulator. Both open loop and closed loop control algorithms are detailed in Section III. The experimental setup and results are reported in Section IV with the conclusions and future work summarized in Section V.

## II. Kinematics

The manipulator used in this study includes two 2-DoF continuum segments connected by a rigid straight segment and stacked on a straight base stem that can be rotated and translated, as presented in [14]. Definitions of the coordinate systems and nomenclature of the manipulator are presented in Section II.A. The forward kinematics and actuation kinematics, which can be referred to a previous study [4], is summarized in Section II.B and Section II.C, respectively.

### A. Coordinate systems and Nomenclature

With the nomenclature defined in Table I, the coordinate systems attached to the $t^{th}$ segment and to the whole manipulator are defined as in Fig. 2.

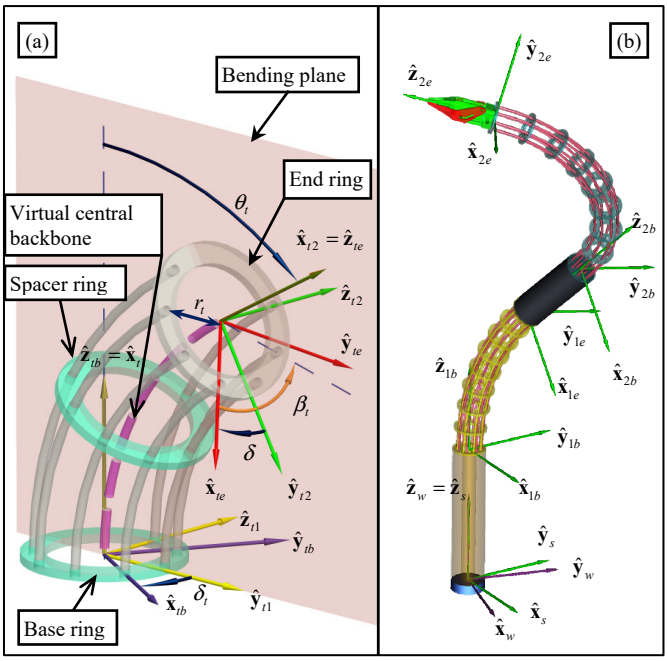


Fig 2. Coordinate systems and nomenclature of: (a) the $t^{th}$ segment, and (b) the whole manipulator.

- The Base Ring Coordinate System (BRCS) $\{tb\} = [\hat{\mathbf{x}}_{tb} \quad \hat{\mathbf{y}}_{tb} \quad \hat{\mathbf{z}}_{tb}]^T$ is attached to the base ring of the $t^{th}$ segment with the xy-plane coinciding with the base ring. The x-axis passes through the first backbone with the origin located at the center of the base ring.
- Bending Plane Coordinate System 1 (BPCS1) $\{t1\} = [\hat{\mathbf{x}}_{t1} \quad \hat{\mathbf{y}}_{t1} \quad \hat{\mathbf{z}}_{t1}]^T$ shares its origin with the BRCS and has its xy-plane coincide with the bending plane of the $t^{th}$ segment.
- Bending Plane Coordinate System 2 (BPCS2) $\{t2\} = [\hat{\mathbf{x}}_{t2} \quad \hat{\mathbf{y}}_{t2} \quad \hat{\mathbf{z}}_{t2}]^T$ has its origin located at the center of the end ring of the $t^{th}$ segment and has its xy-plane coincide with the bending plane of the $t^{th}$ segment.
- End Ring Coordinate System (ERCS) $\{te\} = [\hat{\mathbf{x}}_{te} \quad \hat{\mathbf{y}}_{te} \quad \hat{\mathbf{z}}_{te}]^T$ is attached to the end ring of the $t^{th}$ segment, with the xy-plane coinciding with the end ring. The x-axis passes through the first backbone with its origin shared with the BPCS2.

TABLE I. The Nomenclature Used in This Paper

| Symbol | Definition |
|---|---|
| $t$ | Index of the segments, $t = 1, 2$ |
| $i$ | Index of the backbones, $i = 1, 2, \cdots, m$ |
| $r_t$ | Radius of the pitch circle defining the positions of the backbones in the $t^{th}$ segment. |
| $\beta_{ti}$ | Division angle of the $i^{th}$ backbone in the $t^{th}$ segment. |
| $L_t$ | Length of the imaginary central backbone of the $t^{th}$ segment. |
| $L_n$ | Length of the rigid straight segment. |
| $q_{ti}$ | Push-pull actuation of the $i^{th}$ backbone of the $t^{th}$ segment. |
| $\rho_t$ | The bending radius of the $t^{th}$ segment. |
| $\theta_t$ | The angle indicating the rotation from $\hat{\mathbf{x}}_{t1}$ to $\hat{\mathbf{x}}_{t2}$ about $\hat{\mathbf{z}}_{t1}$. |
| $\delta_t$ | The angle from the bending plane to $\hat{\mathbf{x}}_{tb}$ in the $t^{th}$ segment. |
| $\varphi$ | Axial rotation angle of the base stem. |
| $d$ | Feeding length of the base stem. |
| $\boldsymbol{\Psi}_t$ | $\boldsymbol{\Psi}_t = [\theta_t \quad \delta_t]^T$ is the configuration vector for the $t^{th}$ segment. |
| $\boldsymbol{\Psi}_s$ | $\boldsymbol{\Psi}_s = [\varphi \quad d]^T$ is the configuration vector for the base stem. |
| $\boldsymbol{\Psi}$ | $\boldsymbol{\Psi} = [\boldsymbol{\Psi}_s^T \quad \boldsymbol{\Psi}_1^T \quad \boldsymbol{\Psi}_2^T]^T$ is the configuration vector of the continuum manipulator. |
| ${}^a\mathbf{R}_b$ | Coordinate transformation matrix from frame $\{b\}$ to frame $\{a\}$. |
| ${}^a\mathbf{p}_b$ | Position vector from the origin of the frame $\{a\}$ to the origin of the frame $\{b\}$ in frame $\{a\}$. |
| $\mathbf{J}_{tv}, \mathbf{J}_{tw}$ | Jacobian matrices of linear and angular velocities of the $t^{th}$ segment. $\mathbf{v}_t = \mathbf{J}_{tv}\dot{\boldsymbol{\Psi}}_t$ and $\boldsymbol{\omega}_t = \mathbf{J}_{t\omega}\dot{\boldsymbol{\Psi}}_t$. |

### B. Kinematics of One Segment

For a single continuum segment, its shape is characterized by a virtual central backbone. Verified by theoretical and experimental investigations [15, 16], the constant bending curvature assumption is adopted for the continuum segment, providing a simplified yet accurate description. The forward kinematics of the $t^{th}$ segment is summarized as follows.

Center of the end ring of the $t^{th}$ segment is as follows.

$$ {}^{tb}\mathbf{p}_{te} = \frac{L_t}{\theta_t}\begin{bmatrix} \cos\delta_t(1-\cos\theta_t) \\ \sin\delta_t(\cos\theta_t - 1) \\ \sin\theta_t \end{bmatrix} \tag{1} $$

Where ${}^{tb}\mathbf{p}_{te} = [0 \; 0 \; L_t]^T$ when $\theta_t \to 0$.

The coordinate transformation matrix ${}^{tb}\mathbf{R}_{te}$ relates $\{te\}$ and $\{tb\}$ as in (2).

$$ {}^{tb}\mathbf{R}_{te} = {}^{tb}\mathbf{R}_{t1}\,{}^{t1}\mathbf{R}_{t2}\,{}^{t2}\mathbf{R}_{te} \tag{2} $$

Where

$$ {}^{tb}\mathbf{R}_{t1} = \begin{bmatrix} 0 & \cos\delta_t & \sin\delta_t \\ 0 & -\sin\delta_t & \cos\delta_t \\ 1 & 0 & 0 \end{bmatrix}, {}^{t1}\mathbf{R}_{t2} = \begin{bmatrix} \cos\theta_t & -\sin\theta_t & 0 \\ \sin\theta_t & \cos\theta_t & 0 \\ 0 & 0 & 1 \end{bmatrix}, $$

and $ {}^{t2}\mathbf{R}_{te} = \begin{bmatrix} 0 & 0 & 1 \\ \cos\delta_t & -\sin\delta_t & 0 \\ \sin\delta_t & \cos\delta_t & 0 \end{bmatrix}. $

The instantaneous kinematics for the $t^{th}$ segment is given as follows.

$$ \dot{\mathbf{x}}_t = \begin{bmatrix} \mathbf{v}_t \\ \boldsymbol{\omega}_t \end{bmatrix} = \mathbf{J}\dot{\boldsymbol{\Psi}}_t = \begin{bmatrix} \mathbf{J}_{tv} \\ \mathbf{J}_{t\omega} \end{bmatrix} \begin{bmatrix} \dot{\theta}_t \\ \dot{\delta}_t \end{bmatrix} \tag{3} $$

Where

$$ \mathbf{J}_{tv} = L_t \begin{bmatrix} \cos\delta_t\left(\frac{\sin\theta_t}{\theta_t} + \frac{(\cos\theta_t - 1)}{\theta_t^2}\right) & \frac{\sin\delta_t(\cos\theta_t - 1)}{\theta_t} \\ \sin\delta_t\left(\frac{(1-\cos\theta_t)}{\theta_t^2} - \frac{\sin\theta_t}{\theta_t}\right) & \frac{\cos\delta_t(\cos\theta_t - 1)}{\theta_t} \\ \frac{\cos\theta_t}{\theta_t} - \frac{\sin\theta_t}{\theta_t^2} & 0 \end{bmatrix} \tag{4} $$

$$ \mathbf{J}_{t\omega} = \begin{bmatrix} \sin\delta_t & \cos\delta_t\sin\theta_t \\ \cos\delta_t & -\sin\delta_t\sin\theta_t \\ 0 & \cos\theta_t - 1 \end{bmatrix} \tag{5} $$

### C. Kinematics of the Manipulator

Referring to Fig 2(b), the kinematics for the manipulator is derived from the relationship between the coordinates systems defined in Section II.A. The kinematics is expressed in the world coordinate system.

- The base stem can be rotated and translated along $\hat{\mathbf{z}}_w$. $\{s\}$ is obtained from $\{w\}$ by a rotation of $\varphi$ around $\hat{\mathbf{z}}_w$.
- The first continuum segment is stacked on the distal end of the base stem. $\{1b\}$ is translated from $\{s\}$ by a distance of $d$ along $\hat{\mathbf{z}}_s$.
- The second continuum segment is connected to the first segment with a rigid straight segment in between. $\{2b\}$ is obtained from $\{1e\}$ by a translation of $L_n$. $L_n$ is the length of the rigid straight segment between the two continuum segments.

The kinematics of the manipulator is then parametrized by the configuration vector $\boldsymbol{\Psi} = \begin{bmatrix} \boldsymbol{\Psi}_s^T & \boldsymbol{\Psi}_1^T & \boldsymbol{\Psi}_2^T \end{bmatrix}^T$. The tip position of the manipulator is derived as follows.

$$ {}^{w}\mathbf{p}_{tip} = {}^{w}\mathbf{R}_s\left({}^{s}\mathbf{p}_{1b} + {}^{s}\mathbf{R}_{1b}\left({}^{1b}\mathbf{p}_{1e} + {}^{1b}\mathbf{R}_{1e}\left({}^{1e}\mathbf{p}_{2b} + {}^{1e}\mathbf{R}_{2b}\,{}^{2b}\mathbf{p}_{tip}\right)\right)\right) \tag{6} $$

Where $ {}^{2b}\mathbf{p}_{tip} = {}^{2b}\mathbf{p}_{2e} + {}^{2b}\mathbf{R}_{2e}\,{}^{2e}\mathbf{p}_{tip} $.

According to the structural design, ${}^{s}\mathbf{R}_{1b}$ and ${}^{1e}\mathbf{R}_{2b}$ are identity matrixes.

### D. Actuation Kinematics

The bending of the continuum segment is achieved by pushing and pulling the backbones made from thin nitinol rods. In order to bend the continuum manipulator into a specific configuration, the desired length of the $i^{th}$ backbone in the $t^{th}$ segment is actuated as follows.

$$ q_{ti} = -\theta_t r_t \cos(\delta_t + \beta_{ti}) \tag{7} $$

## III. Control Algorithms

Two control algorithms for the continuum manipulator are described in this section: an open loop one based on the aforementioned kinematics and a closed loop one augmented with a position feedback. Since the closed-form solution of the manipulator's inverse kinematics doesn't exist, differential kinematics is used to construct a resolved motion rates process [17] in both control algorithms.

Flowcharts of both control algorithms are illustrated in Fig. 3. Usually the desired manipulator tip position is attained from a surgeon's input during teleoperated surgery, yet a predefined trajectory is used in this study for consistently evaluating the accuracy.

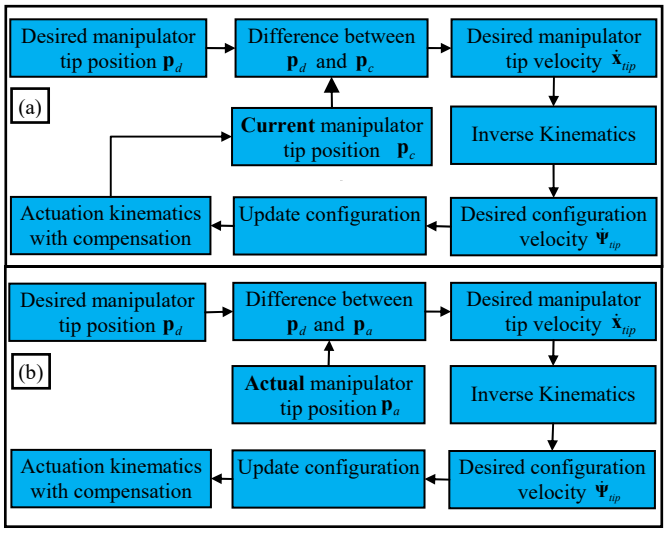


Fig 3. Flowcharts of two control algorithms of continuum manipulator. (a) open loop one and (b) closed loop one.

### A. Open Loop Control Algorithm

As shown in Fig 3(a), when a desired manipulator tip position is input to the control algorithm, the difference between the **desired** tip position $\mathbf{p}_d$ and the **current** tip position $\mathbf{p}_c$ is calculated as in (8). If the length of the difference is smaller than a threshold (in this implementation, 0.1 mm), it is considered that the target position has been reached.

$$ \mathbf{e}_\mathbf{p} = \mathbf{p}_d - \mathbf{p}_c \tag{8} $$

The tip velocity $\dot{\mathbf{x}}_{tip}$ and configuration velocity $\dot{\boldsymbol{\Psi}}_{tip}$ of the manipulator is calculated as (9), (10).

$$ \dot{\mathbf{x}}_{tip} = v_{\lim}\mathbf{e}_\mathbf{p} / \|\mathbf{e}_\mathbf{p}\| \tag{9} $$

Where $v_{lim}$ is the limit velocity determined by the motor' driving ability.

$$\dot{\boldsymbol{\Psi}}_{tip} = \mathbf{J}^{+}\dot{\mathbf{x}}_{tip} \tag{10}$$

Where the singularity robust implementation as in (11) is applied to improve the numerical stability.

$$\mathbf{J}^{+} = \begin{cases} \mathbf{J}^{\mathrm{T}}\left(\mathbf{J}\mathbf{J}^{\mathrm{T}} + \lambda\mathbf{I}\right)^{-1}, \sigma_{\min} < \varepsilon \\ \mathbf{J}^{-1}, \sigma_{\min} \geq \varepsilon \end{cases} \tag{11}$$

Where $\mathbf{J}$ is from (4)(5), $\sigma_{\min}$ is the nonzero smallest singular value, and $\lambda$ and $\varepsilon$ are small positive values ($10^{-4}$ and $10^{-3}$ respectively in this implementation).

Motion calibration is performed in advance and the compensation parameters are obtained from the calibration results. These parameters are then applied to calculate the compensated motor commands.

After the updating of the configuration vector, actuation kinematics calculates the push-pull joint commands and sends them to the motor controllers. In the next servo loop, the current manipulator tip position is updated using the direct kinematics and compared again with new desired tip position.

### B. Closed Loop Control Algorithm

As illustrated in Fig. 3(b), the closed loop control algorithm owns a similar architecture to the open loop one, yet equipped with a real-time tip position feedback. Besides, unlike the open loop control, the compensation parameters in the close loop control can be approximate and shared by different manipulators.

**Actual** manipulator tip position $\mathbf{p}_a$ is measured by an optical tracker in every servo loop. The difference now is calculated between the desired position and the actual position.

$$\mathbf{e}_{\mathbf{p}} = \mathbf{p}_d - \mathbf{p}_a \tag{12}$$

Based on the difference, calculation of desired manipulator tip velocity, inverse kinematics, calculation of the desired configuration velocity, updating of the configuration vector and the actuation kinematics is performed as those in the open loop control. In the next servo loop, the actual manipulator tip position is updated from the tracker and compared again with new desired tip position.

## IV. Experimental Characterizations

In order to validate the effectiveness of the proposed closed loop algorithm, several experiments were carried out. The experimental setup is described in Section IV.A with the experimental methodology explained in Section IV.B. The experimental results are presented in Section IV.C.

### A. Experimental setup

As shown in Fig. 4(a), the continuum surgical manipulator is mounted on an actuation unit and placed on a linear module. A sterile barrier isolates the manipulator from the actuation unit, making the actuation system modular for integration of different manipulators.

Five motors in the actuation unit give manipulator the ability to rotate around its axis and bend the two segments in all directions. The feeding motor in the linear module enables the manipulator to translate along its axis. Hence, the manipulator possesses 6 DoFs.

A RM57 development board (Texas Instrument, Inc) is used to send the motor commands to the motor controllers. It is connected with a laptop (Intel Core i7-4710HQ-2.50GHz, Windows OS x64) via LAN (Local Area Network).

A Polaris Vega optical tracker (Northern Digital, Inc) is used to measure the manipulator's actual tip position. It is connected with the host laptop via LAN, too. The deployment of the tracker is shown in Fig. 4(b). A single NDI passive sphere (Northern Digital, Inc) is attached to the manipulator tip. A marker consisting of four NDI passive spheres is fixed to the manipulator's base, with its local coordinate system predefined.

The sphere's position and the marker's position and orientation with respect to the tracker's coordinate system can be measured by the Vega tracker at a rate of 60 Hz. The sphere's position with respect to the marker's local coordinate system can be calculated. The positions measured by the Vega tracker gives a volumetric accuracy of 0.12 mm RMS. In order to get the latest manipulator tip position in each servo loop, the servo cycle should be longer than the sampling time of the tracker and thus is chosen to be 20 ms.

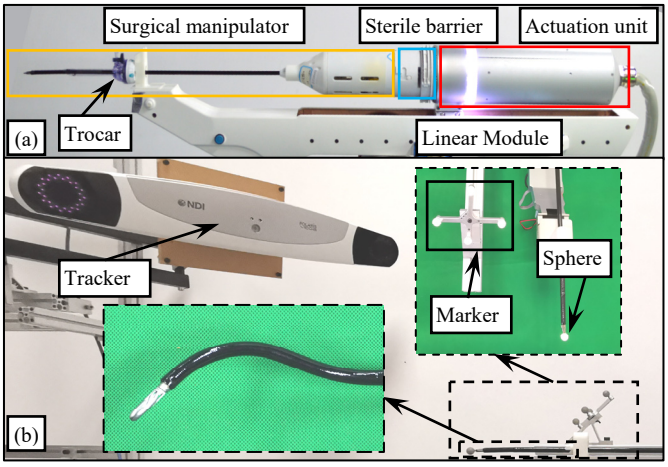


Fig 4. Experimental setup: (a) the continuum surgical manipulator with the actuation unit, (b) the passive sphere is attached to the manipulator's tip and the marker is fixed to the base for optical movements tracking

### B. Experimental Methodology

The goal of the proposed closed loop algorithm is to improve the absolute positioning accuracy of a continuum manipulator, even under unknown external loads. In order to validate the superiority of the closed loop algorithm over the open loop one, the trajectory tracking tasks with different control schemes were performed.

Besides, with the purpose of comparing the absolute positioning accuracy when the manipulator is under significant external force, the same trajectory following tasks were carried out with a 100-gram weight hanging at the manipulator tip, as shown in Fig. 5.

The selected trajectory is to follow a cube with one side parallel to the manipulator's feeding direction. The cube's edge is 80 mm long. The cube center is on the manipulator's feeding axis. The trajectory following velocity is set to a constant value (10 mm/s in this implementation), while decreased to zero as quickly as possible at every vertex.

In order to drive the manipulator tip to follow such a piecewise trajectory, the motors in actuation systems are required to move in a coordinated manner.

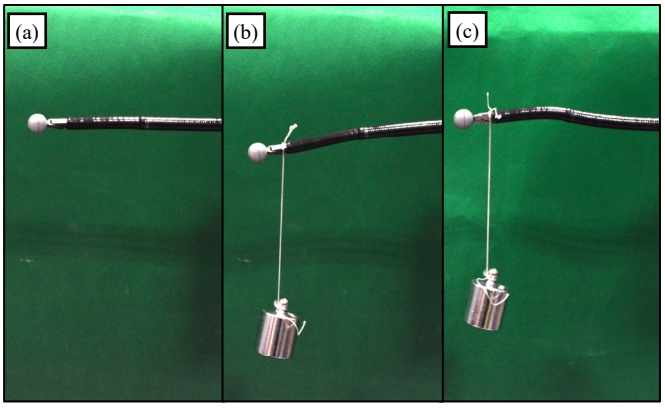


Fig 5. Shape of the surgical manipulatpor in different states: (a) straight manipulator under no load, (b) the open loop control of manipulator under 100-gram weight load, and (c) the closed loop control of manipulator under 100-gram weight load

## C. *Experimental Results*

Compared to the open loop control algorithm, the closed loop one shows great reduction in the absolute positioning errors when the manipulator is under the 100-gram weight. The error is defined as the Euclidean distance between the desired position and the actual position of the manipulator tip.

For the experiment under no load condition, both the target trajectory and the actual trajectories of the manipulator tip positions are plot for comparison in Fig. 6(a), when the control scheme is open loop or closed loop. During the entire procedure, the closed loop control made the manipulator follow the target trajectory well and no distinct motion errors were observed, while there was always evident motion errors between the target trajectory and the trajectory when the open loop control was used.

Moving at a desired velocity of 10 mm/s, introduction of the closed loop algorithm reduces the average error from 4.61 mm to 0.53 mm. Similarly, the maximum error is reduced from 10.96 mm to 2.53 mm.

It's noticeable that there exist small oscillations when the manipulator moves along the x (or y) direction from a stationary state, as shown in Fig. 6(b). No oscillations were observed when the manipulator moved along the Z direction. The reason may be that the motion along the x (or y) direction requires the coordinated movements of the feeding motor and the bending motors. However, the backlashes only existed in the transmission for the bending motors.

Due to the compliance of the continuum surgical manipulator, the manipulator will deform slightly differently under external forces. As shown in Fig 5(b), two continuum segments will bend downward due to the weight hung at the manipulator tip, reducing the accuracy of the tip position. However, using the closed loop control algorithm, the first continuum segment will bend upward to compensate the downward deflection of the second continuum segment, hence reaching the target tip position accurately.

For the experiment under a loaded condition, the trajectories are shown in Fig. 7 with the top view as an inset. The average error was reduced from 16.94 mm to 0.63 mm, and the maximum error was reduced from 21.93 mm to 3.75 mm.

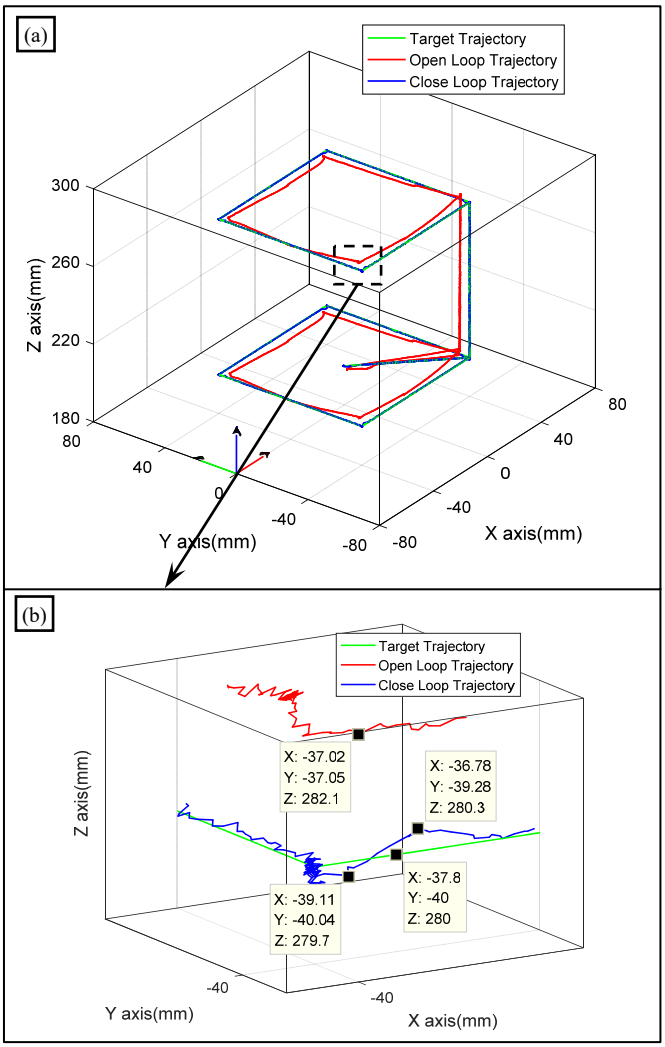


Fig 6. Results of the trajectory following tasks with no payload: (a) the target trajectory and the actual trajectories under the open loop control and the closed loop control; (b) the positioning errors around a vertex

From the top view of the trajectories shown in Fig. 7, the trajectory under the open loop control is biased about 10 mm to the y direction. This is clearly caused by the gravitational force of the weight hung at the manipulator tip.

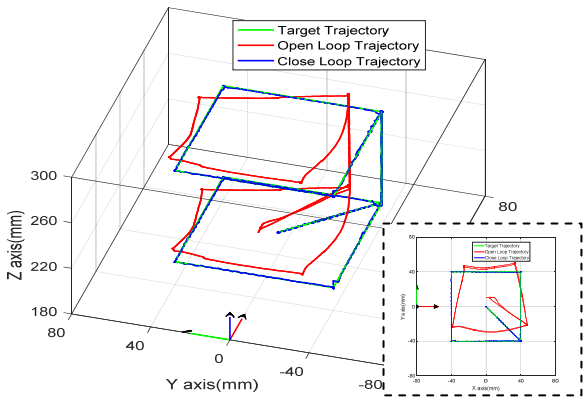


Fig 7. Results of the trajectory following tasks with a 100-gram weight hung at the manipulator tip. Green, red and blue lines represent the target trajectory and the trajectories under the open loop and the closed loop controls

## V. DISCUSSIONS AND CONCLUSIONS

During robotic assisted surgeries, accurate positioning control of the manipulator is crucial to precisely accomplish surgical operational tasks. Due to the lack of shape information, the absolute positioning accuracy of a continuum manipulator can be low. With a vision guidance always applied in laparoscopic surgical robotic systems, visual feedback for tip position provides a way to achieve convenient closed loop control.

A closed loop control algorithm augmented with tip position feedback was proposed in this paper to improve the positioning accuracy. An optical tracking device based on near IR light was adopted in this proof-of-concept investigation, due to the algorithmic complexity and possible feedback accuracy issues from an endoscopic image.

Trajectory following experiments were performed and the results show that the proposed closed loop control algorithm evidently improves the positioning accuracy of the continuum manipulator considerably, especially when the manipulator is under significant external loads. Submillimeter accuracy was achieved with the proposed closed loop control scheme.

In the near future, binocular endoscopic images will be used to replace the near IR tracking system for tip position feedback. Visual markers will be designed and attached to the surgical manipulator, and investigations will be carried out for robust detection of the manipulator tip.

## REFERENCES


[1] R. H. Taylor, "A Perspective on Medical Robotics," *Proceedings of the IEEE,* vol. 94, No.9, pp. 1652- 1664, 2006.

[2] J. Burgner-Kahrs, D. C. Rucker, and H. Choset, "Continuum Robots for Medical Applications: A Survey," *IEEE Transactions on Robotics,* vol. 31, No.6, pp. 1261-1280, Dec 2015.

[3] P. E. Dupont, J. Lock, B. Itkowitz, and E. Butler, "Design and Control of Concentric-Tube Robots," *IEEE Transactions on Robotics,* vol. 26, No.2, pp. 209-225, April 2010.

[4] K. Xu, J. Zhao, and M. Fu, "Development of the SJTU Unfoldable Robotic System (SURS) for Single Port Laparoscopy," *IEEE/ASME Transactions on Mechatronics,* vol. 20, No.5, pp. 2133-2145, Oct 2015.

[5] J. Shang, K. Leibrandt, P. Giataganas, V. Vitiello, C. A. Seneci, P. Wisanuvej, J. Liu, G. Gras, J. Clark, A. Darzi, and G.-Z. Yang, "A Single-Port Robotic System for Transanal Microsurgery - Design and Validation," *IEEE Robotics and Automation Letters,* vol. 2, No.3, pp. 1510-1517, July 2017.

[6] K. Xu and N. Simaan, "Actuation Compensation for Flexible Surgical Snake-like Robots with Redundant Remote Actuation," in *IEEE International Conference on Robotics and Automation (ICRA)*, Orlando, Florida, USA, 2006, pp. 4148- 4154.

[7] N. Simaan, K. Xu, A. Kapoor, W. Wei, P. Kazanzides, P. Flint, and R. H. Taylor, "Design and Integration of a Telerobotic System for Minimally Invasive Surgery of the Throat " *International Journal of Robotics Research,* vol. 28, No.9, pp. 1134-1153, 2009.

[8] R. S. Penning, J. Jung, N. J. Ferrier, and M. R. Zinn, "An Evaluation of Closed-Loop Control Options for Continuum Manipulators," in *IEEE International Conference on Robotics and Automation (ICRA)*, Saint Paul, Minnesota, USA, 2012, pp. 5392-5397.

[9] M. Mahvash and P. E. Dupont, "Stiffness Control of Surgical Continuum Manipulators," *IEEE Transactions on Robotics,* vol. 27, No.2, pp. 334-345, April 2011.

[10] M. C. Yip and D. B. Camarillo, "Model-Less Feedback Control of Continuum Manipulators in Constrained Environments," *IEEE Transactions on Robotics,* vol. 30, No.4, pp. 880-889, 2014.

[11] A. V. Kudryavtsev, M. T. Chikhaoui, A. Liadov, P. Rougeot, F. Spindler, K. Rabenorosoa, J. Burgner-Kahrs, B. Tamadazte, and N. Andreff, "Eye-in-Hand Visual Servoing of Concentric Tube Robots," *IEEE Robotics and Automation Letters,* vol. 3, No.3, pp. 2315-2321, Jul 2018.

[12] X. Ma, C. Song, P. W. Chiu, and Z. Li, "Autonomous Flexible Endoscope for Minimally Invasive Surgery With Enhanced Safety," *IEEE Robotics and Automation Letters,* vol. 4, No.3, pp. 2607-2613, 2019.

[13] M. Azizian, M. Khoshnam, N. Najmaei, and R. V. Patel, "Visual Servoing in Medical Robotics: a Survey. Part I: Endoscopic and Direct Vision Imaging – Techniques and Applications," *The International Journal of Medical Robotics and Computer Assisted Surgery,* vol. 10, No.3, pp. 263-274, 2014.

[14] S. a. Zhang, Y. Chen, Q. Li, B. Zhao, and K. Xu, "Kinematic Optimization of a Continuum Surgical Manipulator," in *IEEE International Conference on Robotics and Biomimetics (ROBIO)*, Kuala Lumpur, Malaysia, 2018, pp. 2069-2074.

[15] R. J. Webster and B. A. Jones, "Design and Kinematic Modeling of Constant Curvature Continuum Robots: A Review " *International Journal of Robotics Research,* vol. 29, No.13, pp. 1661-1683, Nov 2010.

[16] K. Xu and N. Simaan, "Analytic Formulation for the Kinematics, Statics and Shape Restoration of Multibackbone Continuum Robots via Elliptic Integrals," *Journal of Mechanisms and Robotics,* vol. 2, No.011006, pp. 1-13, Feb 2010.

[17] D. E. Whitney, "Resolved Motion Rate Control of Manipulators and Human Prostheses," *IEEE Transactions on Man-Machine Systems,* vol. 10, No.2, pp. 47-53, June 1969.